Superstructure and finite-size effects in a Si photonic woodpile crystal

M. J. A. de Dood,* B. Gralak, and A. Polman
FOM Institute for Atomic and Molecular Physics, Kruislaan 407, 1098 SJ Amsterdam, The Netherlands

J. G. Fleming
Sandia National Laboratories, P.O. Box 5800, Albuquerque, New Mexico 87185

(Received 28 March 2002; revised manuscript received 18 September 2002; published 29 January 2003)

The reflectivity of finite-thickness silicon photonic woodpile structures was measured in the wavelength range from 0.9 to 1.7 μm. Polarization and surface orientation dependent measurements were performed as function of angle of incidence and the data were compared with rigorous calculations for the finite structure. Due to the finite size, the reflectivity near the stop gap edge is strongly orientation and polarization dependent. Clear stop gaps can be identified and good agreement with calculations is found. Outside the stop gap region, Fabry-Perot type resonances are observed that are related to the finite thickness of the photonic crystal. In the stop gap region clear dips are found that are not reproduced in the calculation for perfect, finite-size crystals. These are due an irregularity in the pitch of the woodpile structure as observed in electron microscopy images. This irregularity can be described in terms of a superstructure that introduces additional bands due to zone folding of the bandstructure. Calculations based on the superstructure successfully reproduce the major features in the experimental data.

DOI: 10.1103/PhysRevB.67.035322 PACS number(s): 42.70.Qs,61.72.Bb

I. INTRODUCTION

Photonic crystals are composite dielectric materials, that have a periodic variation in refractive index on a length scale comparable to the wavelength of light. Since their introduction[1,2] these photonic crystals have attracted a lot of attention because of their special optical properties. For sufficiently high index contrast between the materials, photonic crystal structures can be made that do not allow light propagation in any direction in the structure for a limited range of frequencies. This range of frequencies is called the photonic band gap and is commonly investigated by reflection and transmission measurements: no transmission and 100% reflection are expected in the band gap region. Photonic crystals can be used to manipulate optical modes in a controlled way, to modify or inhibit spontaneous emission[1] or to localize light.[2]

For optical and near-infrared wavelengths, photonic crystals require feature sizes of typically 100 nm. Such structures can be made by self-assembly and infiltration techniques[3,4] or by using microfabrication.[5–7] In this article, we will focus on the microfabrication approach. The most amenable structure to microfabrication is a layer-by-layer structure built from layers of parallel dielectric rods (often called a ''woodpile'' crystal). Using high index semiconductor materials this structure can be made using advanced micromachining and integrated circuit processing techniques. This structure has been studied extensively both theoretically[8,9] and experimentally.[5,6,10,11] The photonic band gap in this structure occurs between the first and second bands in the band structure and is thus relatively insensitive to small variations in the structure. Experimentally, the existence of a photonic band gap for near-infrared wavelengths in woodpile crystals has been deduced from reflectivity and transmission measurements both on GaAs (Ref. 6) and Si(Refs. 5,12) structures.

For near-infrared wavelengths existing data report on results with unpolarized light, while experiments with microwaves, on much larger crystals, show a strong polarization dependence.[10,13] Thus, polarization dependent measurements on near-infrared woodpile structures are of great importance. The determination of a photonic band gap at near-infrared wavelengths in an experimentally realizable structure is hampered by the finite number of layers in crystals made by microfabrication techniques. However, both the orientation and termination of the crystal surface are known exactly and this opens the unique possibility to study the effects of polarization and surface orientation in detail.

The photonic crystals in this study are made using the layer-by-layer approach[8,14] and are designed to have a photonic band gap around the important telecommunication wavelength of 1.5 μm. The crystals consist of five layers of stacked poly-crystalline Si bars and their reflective properties have been studied before.[5,12,14] We have done reflectivity measurements on these crystals for different polarizations and surface orientation as function of angle of incidence. The data are compared to calculations done for the finite crystal under study; a comparison that has not been made before. The experimental reflectivity is strongly dependent on both polarization and surface orientation of the crystal. In the stop gap region all data show near 100% reflectivity and good quantitative agreement with calculations is found. Outside the stop gap region, Fabry-Perot type of resonances occur due to the finite thickness. Electron microscopy images indicate that the structure under study is slightly different from the perfect woodpile structure. The experimental structure shows a variation in pitch between alternating rod pairs. A calculation, that includes this imperfection, shows additional features in the reflectivity that exactly match the experimental data. These additional features can be explained in terms of folding of the band structure of a superstructure.

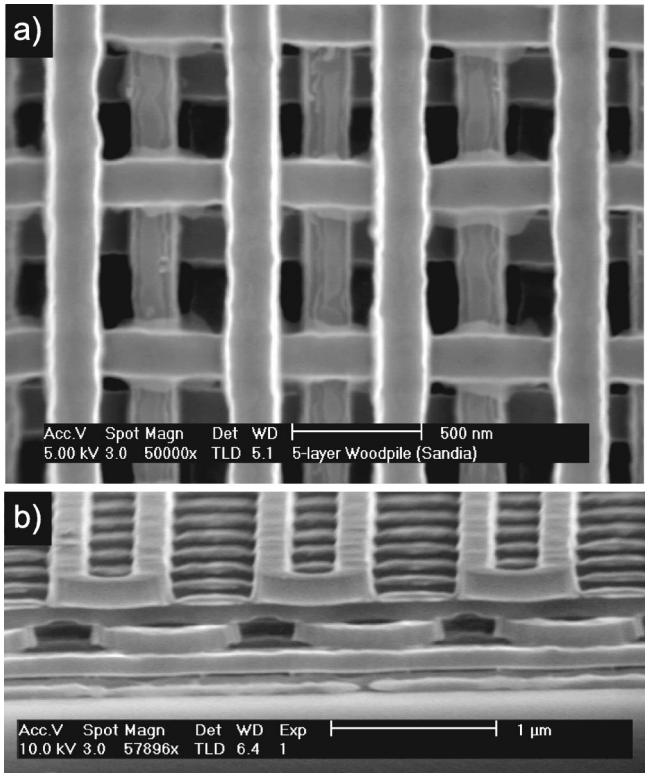

FIG. 1. SEM images of the five-layer woodpile structure, (a) Top view and (b) side view. The rods are 170 nm wide and 200 nm high and the pitch between rods is targeted at 650 nm. As can be seen, there is a variation in the pitch between alternating rod pairs caused by the filet process. However, the sum of two adjacent pitches is always 1300 nm.

II. EXPERIMENTAL STRUCTURE

Photonic crystals are fabricated from polycrystalline Si (p-Si) using lithography and ion etching techniques according to a layer-by-layer design, developed for Si by Lin and Fleming.[8,14] The design uses layers of parallel one-dimensional rods of rectangular cross section. The layers are stacked such that the orientation of the rods on alternate layers is rotated by 90°. Between every two layers, the rods are displaced relative to each other by exactly half the pitch between the rods. In this way a structure is built that repeats itself every four layers and has a face-centered-tetragonal lattice symmetry. The crystals described in this work are composed of p-Si bars with a width of 170 nm and a height of 200 nm. The pitch between rods is $\sim$650 nm and the crystal in this study consists of five layers of stacked parallel rods. The volume fraction of dielectric (p-Si) is 0.28 in this case. The crystal is designed to have a complete photonic band gap including the important telecommunication wavelength of 1.5 μm. Si is transparent at this wavelength and is thus well suited since it provides a high index contrast [$n = 3.45$ at $\lambda = 1.5\mu$m (Ref. 15)]. Figure 1 shows scanning electron microscopy (SEM) images of the crystals used in this study, looking from the top (a) and under an angle of 80° (b). The individual rods of p-Si are clearly visible in Fig. 1 which shows both the 90° rotation of alternate layers [Fig. 1(a)] and the displacement by half the pitch between every two layers [Fig. 1(a) and (b)].

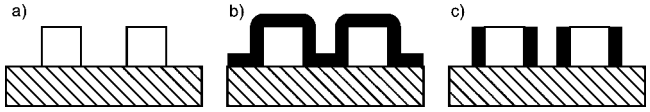

FIG. 2. Schematic representation of the essential steps in the filet process (cross section). (a) Definition of an array of SiO_2 bars on a p-Si layer (hatched area). (b) The bars are covered with a thin p-Si layer. (c) After anisotropic etching of the structure in (b) a thin sliver of p-Si material remains at the sidewall. The thickness of these slivers is equal (or at least proportional) to the thickness of the deposited layer. The slivers then serve as a mask for etching the underlying p-Si layer, and are much smaller than the originally patterned structure in (a).

The photonic crystal is fabricated on a 6 inch Si wafer using advanced silicon processing developed for the fabrication of microelectro-mechanical systems and integrated circuits. First a $\sim$70 nm thick silicon nitride film is deposited on the substrate, followed by low-pressure chemical vapor deposition of a p-Si layer. The p-Si is then patterned to define the first layer of parallel rods. This requires the fabrication of feature sizes down to 170 nm and is achieved using a filet process as described in detail elsewhere.[14] The essential steps are depicted in Fig. 2. In a filet process the minimum feature size is determined by sidewall coverage of a deposited thin film. In this filet process first a structure is defined that has a relatively large feature size [Fig. 2(a)]. Next, a thin film of p-Si is deposited over the structure [Fig. 2(b)] and then subjected to isotropic reactive ion etching. As a result a thin sliver of p-Si remains on the sidewalls of the SiO_2 bars [Fig. 2(c)]. If the bar height is several times greater that the thickness of the deposited film, then the width of the filet is equal (or at least proportional) to the film thickness. Using this procedure thus relaxes the requirements on the photopatterning, since the minimum feature size equals the pitch in between the rods (650 nm). After removing the SiO_2 bars, the remaining p-Si slivers are used as a mask for ion etching an underlying p-Si film.

After etching, the open space in between the rods is filled with SiO_2 and the layer is planarized and polished using chemical-mechanical polishing (CMP). The planarization step is critical, since this prevents the topography generated in the first level from being replicated in the subsequent level. After CMP of the first layer a second layer of p-Si is deposited and patterned. The entire process is repeated until five layers of rods are fabricated. After completion of the entire structure the SiO_2 is removed by selective wet etching.

As can be seen in Fig. 1 there is a slight variation in pitch between alternating rod pairs within each layer, which is a result of the filet process. However, the sum of the two adjacent pitches is always exactly 1300 nm and is defined by the pitch of the SiO_2 bars used in the filet process. Note that this variation in pitch is not intrinsic to the filet process or other Si processing techniques in general. In principle, the variation in pitch observed here can be avoided with relative ease. The typical U-shaped profiles visible in Fig. 1(b) occur at the edges of the crystal and are a consequence of the filet

process as well. The individual crystals on the wafer are 2 $\times 2$ mm in size and the rods have the same alignment in all crystals covering the 6 inch diameter wafer. While the thickness of the crystals is finite (five layers) the in-plane structure can be considered as infinite.

III. NUMERICAL METHOD AND MODEL

To calculate the spectral reflectivity of these finite woodpile crystals, a numerical method is employed that is based on the generalization of the method of ''exact eigenvalues and eigenfunctions'' used in the study of lamellar gratings.[16–18] The woodpile structure under consideration can be described as a stack of gratings. Using this method, the dielectric function is represented exactly and the electromagnetic field in each layer of rods (grating) is expanded in a suitable basis of ''exact eigenfunctions.'' In this way, convergence problems associated to Gibbs phenomena in a Fourier approximation (plane wave method) are avoided. Next, the stable *R* algorithm, developed by Li *et al.*,[19] is used to obtain an expansion of the electromagnetic field in a stack of several grating layers. Finally, the electromagnetic fields in the homogeneous media above and below the stack of layers are expanded in a Fourier basis. In the far field, reflection and transmission of the incident wave are given by the reflected and transmitted fractions of the Poynting vector of the incident wave.

The structure modeled is identical to that described in the experimental section and is built up from layers of parallel rods of rectangular cross section. The rods are assumed to be nonabsorbing *p*-Si with a (wavelength independent) refractive index of 3.45 [index of crystalline Si at $\lambda = 1.5$ μm. (Ref. 15)] Convergence of the calculations was verified by extending the number of eigenfunctions in the expansion, as reported in. Ref. 20 Since there is no absorption, energy conservation can also be checked by comparing the sum of the calculated transmission and reflection to the flux of the Poynting vector of the incoming plane wave. The observed difference is always less than 3%.

In this work we are mainly interested in the reflected field. The incident plane wave is characterized by the angle of incidence θ relative to the surface normal of the sample. The polarization of the incident plane wave can be specified and is either *s* or *p* polarized. Also, the angle between the scattering plane and the long axis of the first row of rods (the sample azimuth) is specified. Thus, for each given angle of incidence four different reflectivity (and transmitivity) curves can be calculated.

The calculations are first done assuming an ''ideal'' crystal (i.e., without the superstructure observed in Fig. 1) based on the experimentally determined dimensions of the *p*-Si bars. In each layer the bars are 170 nm wide and 200 nm high and are placed on a pitch of 650 nm. The superstrate is air with a refractive index of 1.0. The substrate is modeled by an infinite layer of crystalline Si with $n = 3.45$. To model the structure correctly a homogeneous (unstructured) silicon nitride layer ($n = 2.0$) of 70 nm thickness is inserted in between the Si substrate and the five-layer woodpile structure. The thickness of this layer, that was inserted as a buffer layer between the Si substrate and the woodpile structure, was determined using Rutherford backscattering spectrometry (not shown). The substrate can be modeled as being infinite since the backside of the supporting Si wafer is unpolished.

IV. REFLECTIVITY MEASUREMENTS AND DISCUSSION

To probe the optical properties of the photonic crystal, the polarization dependent reflectivity was measured using a variable angle spectroscopic ellipsometer. White light from a Xe lamp was first led through a grating monochromator and then illuminates the sample under study with a parallel beam with a diameter of 1 mm. The angle of incidence, measured relative to the surface normal, can be varied between 20° and 80°. The reflected light was collected using a combined Si and Ge photodiode, covering the spectral range from 300 to 1700 nm. The incident beam is fixed, while the sample stage and detector rotate using a $\theta - 2\theta$ geometry. Polarization dependent measurements are done using two polarizers. One polarizer is mounted in the input beam to illuminate the sample with linearly polarized light. A second linear polarizer is mounted in front of the detector and analyzes the polarization of the reflected light. The extinction ratio of the polarizers is at least 30 dB. Reflectivity measurements are obtained by first measuring the (linearly polarized) white light spectrum of the lamp in a straight-through configuration. Next, the reflected light from the photonic crystal under study is measured. The reflectivity of the sample is then calculated by dividing the reflected intensity from the sample by the reference intensity of the lamp at each wavelength. The absolute accuracy of the reflectivity determined in this way is better than 10%.

The alignment of the first layer of rods on the surface relative to the scattering plane was verified by measuring the reflectivity for crossed polarizations, i.e., the incident light is *p* polarized and the detector is configured to measure *s*-polarized light (or vice versa). On symmetry grounds the reflectivity for crossed polarization should be zero; experimentally this typically amounts to less than 3% (alignment is better than 2°). Figures 3 and 4 show the measured (drawn lines) and calculated (dashed lines) reflectivity spectra of the five-layer photonic woodpile lattice at an angle of incidence $\theta = 20°$. Data are shown for *s* and *p* polarized light, as indicated by the *s* and *p* symbols in the figures. Figure 3 shows data for a crystal with the long axis of the first layer of rods aligned perpendicular to the scattering plane (defined by incoming and outgoing wave vectors). Measurements on the same sample, but with the long axis aligned in the scattering plane are shown in Fig. 4. The schematic above each figure shows the incoming and outgoing wave vectors of the light and a cross section of the woodpile defining the surface orientation. As can be seen in Figs. 3 and 4, all four possible combinations of surface orientation and polarization yield quite different reflectivity spectra.

Figures 3 and 4 show that for wavelengths longer than ~ 1.5 μm the reflectivity is near 100% for all four geometries, consistent with the calculated photonic stop gap at $\theta = 20°$.[8] The observed stop gap extends into the infrared, well beyond the experimental limit of 1.7 μm, as expected from

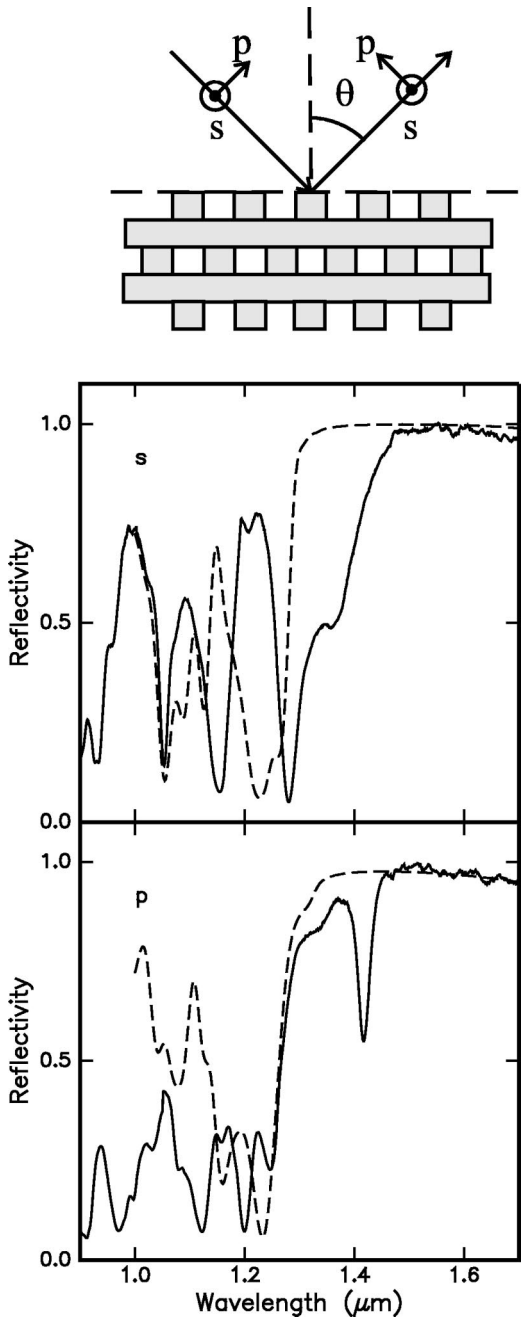

FIG. 3. Reflectivity spectra of the photonic woodpile lattice for *s* (top) and *p* (bottom) polarized light. The angle of incidence is $\theta = 20°$ and the long axis of the first row of rods is aligned perpendicular to the scattering plane. Both experimental data (drawn line) and calculated data (dashed line) are shown. The calculated data assume an ideal finite structure (see text).

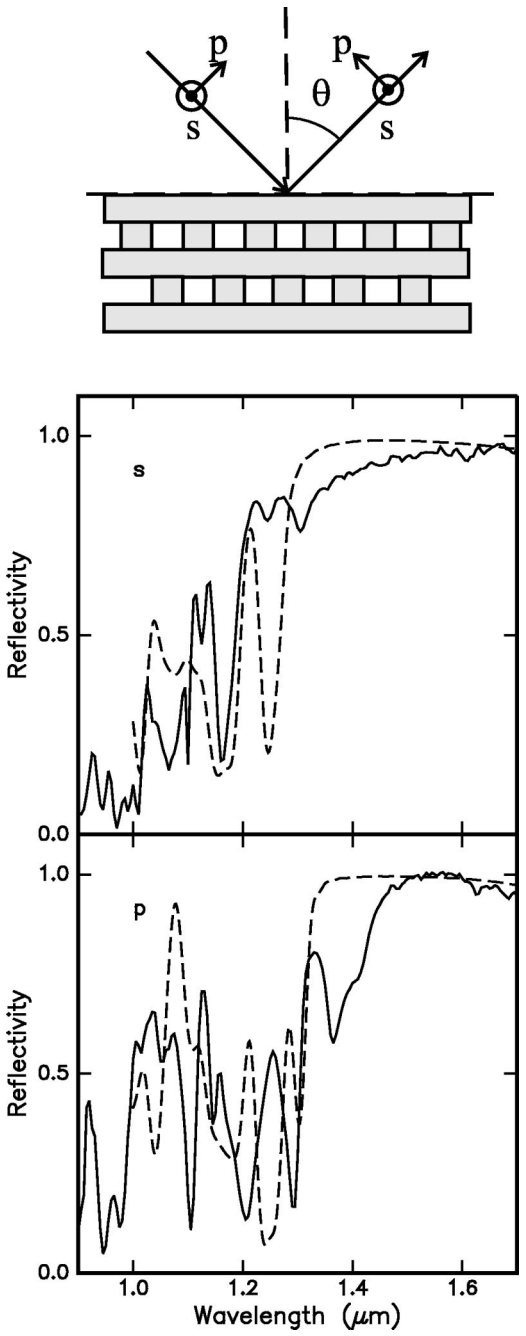

FIG. 4. Reflectivity spectra of the photonic woodpile lattice for *s* (top) and *p* (bottom) polarized light. The angle of incidence is $\theta = 20°$ and the long axis of the first row of rods is aligned parallel to the scattering plane. Both experimental data (drawn line) and calculated data (dashed line) are shown. The calculated data assume an ideal finite structure (see text).

both our calculations and experiments with unpolarized light.[5] Comparing the measured reflectivity (drawn lines) and calculated values (dashed lines), good agreement is achieved for all four measurements in the region $\lambda > 1.5$ μm. The measured position of the short wavelength edge of the stop gap (defined as $R = 50\%$) agrees well with calculations for *p*-polarized light, although the dips at ~ 1.41 μm (Fig. 3) and ~ 1.35 μm (Fig. 4) are not reproduced in the calculation. For *s*-polarized data the agreement is less satisfactory.

For wavelengths < 1.2 μm, a low reflectivity is observed since at these wavelengths no photonic stop gap exists and light can propagate in the photonic crystal. The structure in the spectra at shorter wavelengths is the result of Fabry-Perot type of resonances due to the finite thickness of the crystal. Note that in the wavelength range down to 1.15 μm (electronic band gap of bulk Si) Si is fully transparent. For wavelengths down to 0.9 μm Si is only weakly absorbing (ab-

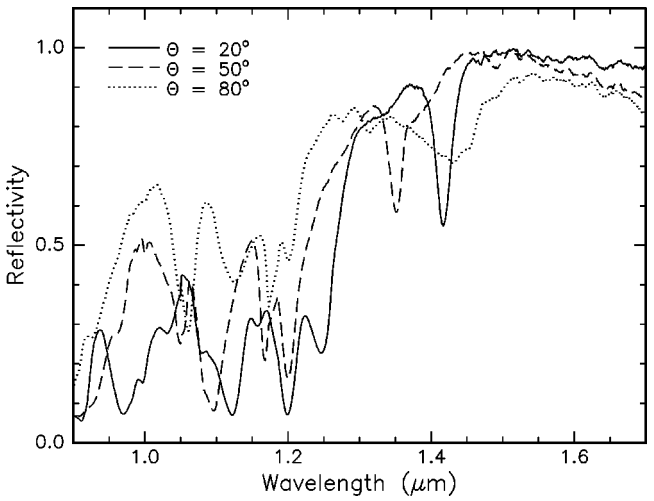

FIG. 5. Reflectivity spectra of the photonic woodpile lattice for *p* polarized light for three different angles of incidence. The long axis of the first row of rods is aligned perpendicular to the scattering plane. A clear shift of the ''band edge'' towards shorter wavelength is observed with increasing angle.

sorption length $\sim 30\ \mu$m). Thus the comparison with calculations (that do not include absorption) is a valid one. For wavelengths below 0.9 μm, the specular reflectivity decreases (not shown), which can be explained by a combination of diffraction and absorption by the Si in that spectral range.

In order to achieve better agreement between measured and calculated data both the width of the *p*-Si bars and the thickness of the silicon nitride buffer layer were adjusted. The width of the *p*-Si bars was varied from 180 to 170 nm. It was found that decreasing the width of the bars leads to a shift of the band edge towards longer wavelength. This shift of the band edge is a combined effect of a shift of the midgap wavelength towards shorter wavelength, and changes in both the relative gapwidth and the Fabry-Perot resonances. The silicon nitride layer thickness was varied from 0 to 70 nm. Changing the silicon nitride thickness modifies the resonances in the short wavelength region due to a change in both the amplitude and the relative phase of the wave reflected by the substrate. The best agreement between calculated data and experiment is found for the calculations in Figs. 3 and 4, that use 170 nm wide bars and a 70 nm thick silicon nitride buffer layer (see experimental section). Our data demonstrate that in particular at and below the band gap region polarization is a key parameter determining the optical response of the photonic woodpile crystal.

Next, we discuss the angle dependence of the reflectivity for polarized light in order to experimentally determine the band gap edge. So far, for optical and near-infrared wavelengths, experiments were only done using unpolarized light.[5,12] Our data described above demonstrate that this is a severe limitation (see Figs. 3 and 4). Our data clearly shows a large stop gap at $\theta = 20°$, but these data confirm nor exclude the existence of a full photonic band gap (i.e., stop gap in all direction). Figure 5 shows measured reflectivity spectra for three different angles of incidence (20°, 50°, and 80°).

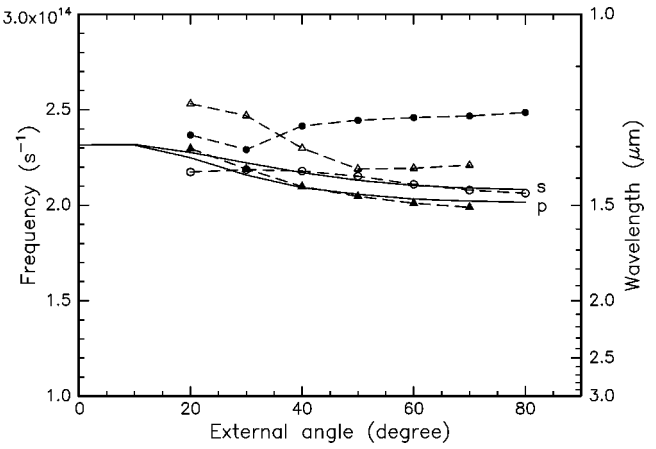

FIG. 6. ''Dispersion'' curves $\omega(k_\parallel)$ obtained from reflectivity data as function of angle of incidence. The low-wavelength (high-frequency) stop gap edge is shown for *p* polarization (solid symbols) and *s* polarization (open symbols). The different surface orientation are studied: (△,▲) indicate that the long axis of the first row of rods is in the scattering plane, (○,●) indicate that the long axis of the first row of rods is perpendicular to the scattering plane. The dashed lines connect the experimental data points and serve to guide the eye. The drawn line shows the band edges calculated as function of external angle, obtained from a calculation on a thick crystal (32 layers). The *s* and *p* labels indicate *s* and *p* polarization for the theoretical curves.

The reflectivity is measured for *p* polarized light, with the sample aligned such that the long axis of the first layer of rods is perpendicular to the scattering plane (see schematic of the geometry in Fig. 3). The reflectivity for wavelengths between 1.5 and 1.7 μm is close to 100% for all angles of incidence and a shift of the edge of the stop gap towards shorter wavelength (higher frequency) is observed for increasing angle. Clear dips in the reflectivity data are observed at $\lambda = 1.35$ and 1.42 μm for angles of incidence of 20° (as in Fig. 3) and 50° respectively. These dips are not reproduced by the calculation, as will be discussed later. The much broader feature around $\lambda = 1.4\ \mu$m for an angle of incidence of 80° is also found in the calculations and has a different origin than the sharp dips observed for 20° and 50°.

Reflectivity measurements, similar to those in Fig. 5 were done for both polarizations and surface orientations. The angle of incidence ranged from 20° to 80°. At each angle the position of the stop gap was estimated by determining the wavelength at which the reflectivity drops below 50%. The experimental results are summarized in Fig. 6. Data are shown for both *p* polarization (solid symbols) and *s* polarization (open symbols). The different orientations of the first layer of rods relative to the scattering plane are indicated. Open and closed circles symbols indicate that the long axis of the first row of rods is perpendicular to the scattering plane. Open and closed triangles indicate that the long axis of the first row of rods is in the plane of measurement. The dashed lines connect the experimental data points and serve to guide the eye. As can be seen in Fig. 6 all four combinations of polarization and surface orientation lead to a different stop gap edge.

The data in Fig. 6 are compared to the calculated stop gap

edge of a 32 layers thick crystal (drawn lines) as function of external angle. Calculations are shown for the two polarizations and are different because the coupling of the incoming plane wave to the crystal is different for the two polarizations. No difference is found for near-normal incidence as expected on symmetry grounds. In the calculations, the position of the calculated band edge as function of external angle was found to be independent of the surface orientation. This is expected, since for an infinite crystal the two orientations cannot be distinguished. Model calculations show that the effect of increasing the crystal thickness on the reflectivity is twofold; the reflectivity in the stop gap regions further increases towards 100% and the edges of a photonic stop gap become sharper. Hence, from such a calculation the stop gap edge can be determined unambiguously.

Note that the ''dispersion'' curves in Fig. 6 are plotted as function of external angle, while a band structure is specified as function of Bloch wave vector inside the crystal. The conversion can be made using Snell's law, i.e., the wave vector component in the direction parallel to the interface is conserved $[k_{\parallel}=(2\pi/\lambda)\sin\theta]$. The perpendicular component of the wave vector propagating in the crystal is determined by the band structure.

As can be seen in Fig. 6 good agreement between the calculation and experimental data is observed for *p* polarized light with the long axis of the rods in the scattering plane (▲ data) and for *s* polarized light with the long axis of the rods perpendicular to the scattering plane (○ data). In these two cases the long axis of the first, third and fifth layers of rods is aligned with (a component of) the *E* field of the incoming light. Since rods are easily polarized when the *E* field is in the direction of the long axis, the light effectively interacts with three layers. For the remaining two geometries, the agreement is less good, because in this case the *E* field is aligned with the long axis of the rods for only two layers.

Based on band structure calculations that support the existence of a photonic band gap for the present woodpile structure and the correspondence of calculated and experimental results in Fig. 6, we conclude that our data support the existence of a full photonic band gap in these woodpile crystals (for an infinite crystal). The discrepancies between calculated and experimental data are due to the finite size of the crystal. In addition, the dips in the experimental reflectivity, unexplained by the theory discussed so far, make the determination of the band edge less accurate. The remainder of this article discusses the origin of these dips and their influence on the band gap in detail.

Measurements and theory on woodpile photonic crystals have mostly concentrated on perfect structures. However, experimentally such crystals do not exist. In fact, a careful observation of the SEM images in Fig. 1 reveals a variation in pitch that finds its origin in the nature of the filet process (see Fig. 2). So far, only a limited amount of work is done to understand the effects of disorder on the photonic band gap of woodpile structures.[21,22] The imperfections considered typically shift or change the rods in the unit cell and thereby repeat the defect leaving the entire structure still periodic. The effect of such imperfections can be calculated, since this involves a calculation of the band structure of a photonic crystal with a different unit cell (in our case a four times bigger unit cell is needed). Note that a clear distinction should be made between the periodic imperfections as found here, and that may lead to propagating (Bloch) modes, and random defects or disorder, that lead to localized states.

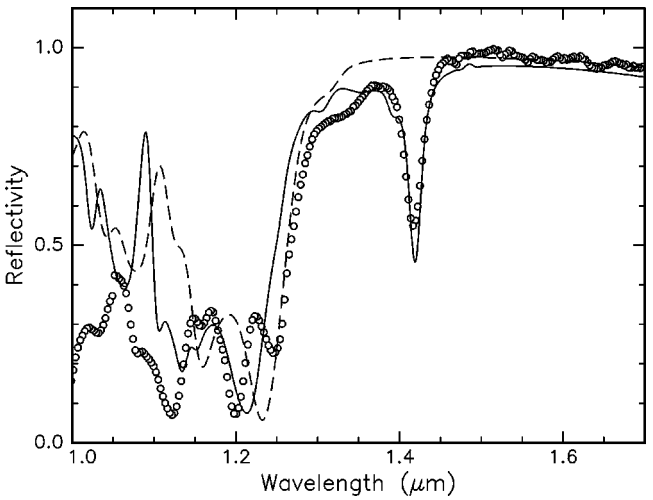

FIG. 7. Reflectivity spectra of the woodpile structure for *p*-polarized light at an angle of incidence of 20°. Experimental data (○) are compared to calculations of a perfect structure (dashed line) and structure that includes the experimentally determined superstructure in the (five-layer) crystal (drawn line). The calculation of the slightly perturbed structure gives a satisfactory description of the dip in the reflectivity at $\lambda=1.42$ μm.

From the SEM images in Fig. 1 it is found that the pitch between alternating rod pairs is not constant in all layers of the structure. The pitch between rods alternates between 600 and 700 nm and creates a superstructure with a pitch of 1300 nm in both directions. Figure 7 shows the measured reflectivity (○) at an angle of incidence $\theta=20°$, for *p*-polarized light. The long axis of the first layer of rods is perpendicular to the scattering plane [same data as in Fig. 3(b)]. Overlaid on the measurements are calculations of the reflectivity for two cases: a perfect structure [dashed line, same as in Fig. 3(b)], and a calculation using the technique described in Sec. III that takes the variation in the pitch into account (drawn line). As can be seen, the distinct dip in the experimental data at 1.42 μm is very well reproduced by the calculation.

The origin of the dip in the spectra can be explained as follows. The structure that has a variation in pitch in both in-plane directions can be described using an unit cell (in real space) that is exactly twice as large as that of the ''ideal'' structure. As a consequence, the irreducible part of the Brillouin zone (in reciprocal space) of this superstructure is twice as small in both directions. An approximate band structure of this structure can be obtained by a single folding of the band structure of the ''ideal'' crystal in both directions. The result of this zone folding is that modes that exist on the edge of the Brillouin zone for a perfect crystal fold back to the center of the Brillouin zone in the case of the superstructure. In the perfect structure, modes from the second band are generally at lower energies (longer wavelength) at the edge of the Brillouin zone. The folding thus introduces the possibility of propagating modes in the stop gap region and is thus

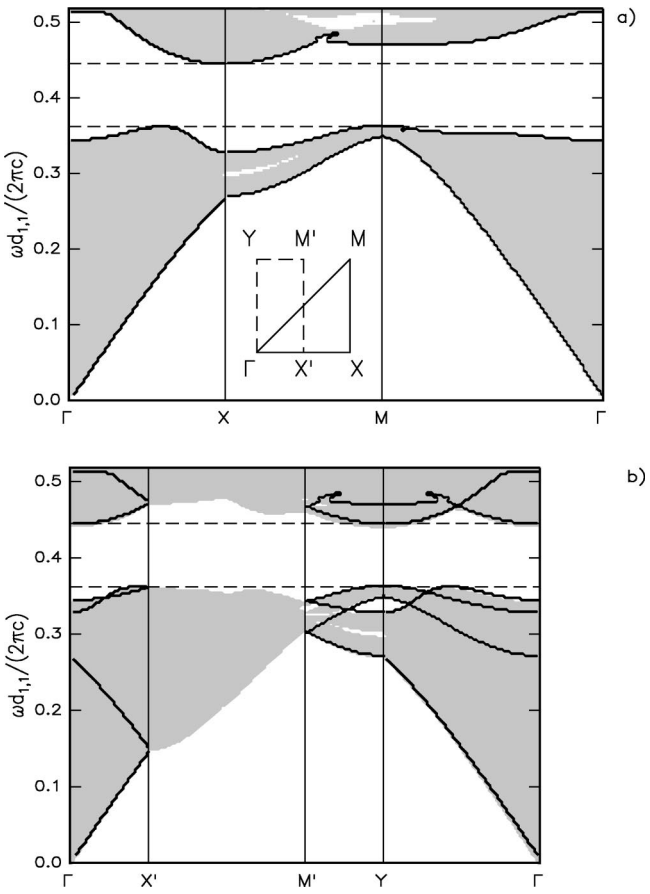

FIG. 8. Representation of the calculated dispersion relation for the perfect layer-by-layer structure (a) and for a crystal with a periodic variation in pitch (b). The white regions indicate the region where no solution exists; the gray area indicates the existence of a solution. The black lines in (a) indicate the edge of the gray region for the perfect crystal. The black lines in (b) were constructed from the lines in (a) by a single zone folding.

consistent with the observed dip in the reflectivity at $\lambda = 1.42\ \mu$m in Fig. 7. Figure 5 shows that this dip shifts towards shorter wavelength for increasing angle of incidence as anticipated by the zone folding argument (the shift of the dip with incident angle is consistent with the dispersion of modes that are folded back). Note that this argument only explains the possible existence of modes and is not sufficient to explain the dip as that requires consideration of coupling to these modes and taking into account the finiteness of the structure. To reproduce the dip in the reflectivity a rigorous calculation, is needed that includes both the coupling to the modes and the finiteness of the structure. This calculation is presented in Fig. 7. The remaining difference between calculation and experiment might be further improved by including the effect of index dispersion of the Si in the calculation.

To better illustrate the concept of a single zone folding we have calculated the band structure for a perfect layer-by-layer structure [Fig. 8(a)] and compared it to the band structure of a layer-by-layer structure that has a periodic variation in the pitch in one direction only [Fig. 8(b)]. The periodic variation was considered in one direction only to reduce the computational effort and to better clarify the folding. The band structure is plotted as function of the k vector projected on the two-dimensional plane defined by the layer-by-layer structure. The gray and white areas indicate the existence (gray) or absence (white) of a solution for a specific combination of the in-plane k vector and frequency ω. Figure 8(a) reveals that the perfect structure has a full photonic band gap from $\omega d_x/(2\pi c) = 0.362$ (M point) to $\omega d_x/(2\pi c) = 0.445$ (X point). A more detailed description of the method and the special representation of the dispersion relation can be found in Ref. 20.

The black lines in Fig. 8(a) indicate the boundary of the gray area of the perfect structure. The gray and white areas in Fig. 8(b) indicate the calculated band structure for a layer-by-layer structure that has a periodic variation in one direction. The black lines in Fig. 8(b) are obtained by a single folding procedure from the black lines of Fig. 8(a). This zone folding was done by considering the irreducible part of the Brillouin zone for the in plane k vector. These irreducible parts are shown in the inset of Fig. 8(a). From this inset one can deduce that the band structure in the ΓY direction contains contributions from the ΓX (in the perfect, symmetric, case the X and Y points are the same) and XM direction (due to folding) of the perfect structure, while the $\Gamma X'$ and YM' are folded versions of the ΓX and XM (in the perfect, symmetric, case the X and Y points are the same) band structure. As can be seen from Fig. 8(b), very good agreement between the folded band structure (black lines) and the full band structure calculation (gray and white area) is obtained. Note that the position and size of the band gap is not changed by this zone-folding process. From these calculations we conclude that our zone-folding argument is indeed a valid one.

V. CONCLUSIONS

Polarization and surface orientation dependent reflectivity spectra was measured on a Si photonic woodpile structure of finite thickness. The reflectivity was found to depend strongly on both polarization and surface orientation. In the stop gap region the reflectivity reaches a value close to 100% independent of polarization or surface orientation. A direct comparison between experimental data and calculations confirms the existence of photonic stop gaps. Comparing the experimentally determined stop gap edges with calculations yields good agreement for two combinations of polarization and sample azimuth. In the other two cases the agreement is less satisfactory. The agreement is best for measurement conditions that have a component of the E field aligned with the first layer of rods, effectively increasing the interaction with the five-layer crystal. The calculated position of the band edge for a 32 layer thick crystal was independent of surface orientation of the first layer. Hence, a measured orientation dependence is a result of the finite thickness of the crystal.

At shorter wavelengths, outside the stop gap region, the structure observed in the reflectivity data is a result of Fabry-Perot type resonances related to the finite thickness of the photonic crystal under study. These resonances depend on the vertical component of the Bloch-wave vector in the struc-

ture and are sensitive to small changes in the structure. Experimentally it was observed that the photonic woodpile structure has a variation in pitch, which introduces a superstructure. This superstructure was introduced in the calculation and results in better agreement with experimental data. In particular a distinct dip observed in the experimental reflectivity spectra is successfully reproduced by the calculation. To origin of the dip was explained in terms of new bands introduced in the band structure described by zone folding of the band structure. This zone folding was illustrated by comparing calculated band structures for a perfect structure with those of a structure that has a periodic variation in pitch in one direction.

ACKNOWLEDGMENTS

The silicon photonic lattices were fabricated at Sandia National Laboratories' Microelectronics Development Laboratory (MDL). The process and design was guided by Dr. Shawn-Yu Lin, also of Sandia National Laboratories. Sandia is a multiprogram laboratory operated by Sandia Corporation, a Lockheed Martin Company, for the United States Department of Energy under Contract No. DE-AC04-94AL85000. This work is part of the research program of the Foundation for Fundamental Research on Matter (FOM) and was made possible by financial support from the Dutch Foundation of Scientific Research (NWO).

*Email address: mdedood@physics.ucsb.edu
Present address: California Nanosystems Institute, University of California Santa Barbara, Santa Barbara, CA 93106.

[1] E. Yablonovitch, Phys. Rev. Lett. **58**, 2059 (1987).
[2] S. John, Phys. Rev. Lett. **58**, 2486 (1987).
[3] J.E.G.J. Wijnhoven and W.L. Vos, Science **281**, 802 (1998).
[4] A. Blanco, *et al.*, Nature (London) **405**, 437 (2000).
[5] S.-Y. Lin, J.G. Fleming, D.L. Hetherington, B.K. Smith, R. Biswas, K.M. Ho, M.M. Sigalas, W. Zubrzycki, S.R. Kurtz, and J. Bur, Nature (London) **394**, 251 (1998).
[6] S. Noda, K. Tomoda, N. Yamamoto, and A. Chutinan, Science **289**, 604 (2000).
[7] C.C. Cheng, A. Scherer, V. Arbet-Engels, and E. Yablonovitch, J. Vac. Sci. Technol. B **14**, 4110 (1996).
[8] K.M. Ho, C.T. Chan, C.M. Soukoulis, R. Biswas, and M. Sigalas, Solid State Commun. **89**, 413 (1994).
[9] H.S. Sozuer and J.P. Dowling, J. Mod. Opt. **41**, 231 (1994).
[10] E. Özbay, A. Abeyta, G. Tuttle, M. Tringides, R. Biswas, C.T. Chan, C.M. Soukoulis, and K.M. Ho, Phys. Rev. B **50**, 1945 (1994).
[11] M.C. Wanke, O. Lehmann, K. Müller, Q. Wen, and M. Stuke, Science **275**, 1284 (1997).
[12] S.-Y. Lin and J.G. Fleming, J. Lightwave Technol. **17**, 1944 (1999).
[13] E. Yablonovitch, T.J. Gmitter, and K.M. Leung, Phys. Rev. Lett. **67**, 2295 (1991).
[14] J.G. Fleming and S.-Y. Lin, Opt. Lett. **24**, 49 (1999).
[15] E.D. Palik, *Handbook of Optical Constants of Solids* (Academic Press, Boston, 1991), Vol. 2.
[16] *Electromagnetic Theory of Gratings*, edited by R. Petit, (Springer Verlag, Berlin, 1980).
[17] L.C. Botten, M.S. Craig, R.C. McPhedran, J.L. Adams, and J.R. Andrewartha, Opt. Acta **28**, 413 (1981).
[18] L. Li, J. Mod. Opt. **40**, 553 (1993).
[19] L. Li, J. Opt. Soc. Am. A **13**, 1024 (1996).
[20] B. Gralak, S. Enoch, and G. Tayeb, J. Opt. Soc. Am. A **19**, 1547 (2002).
[21] S. Ogawa, K. Tomoda, and S. Noda, J. Appl. Phys. **91**, 513 (2002).
[22] A. Chutinan and S. Noda, J. Opt. Soc. Am. B **16**, 240 (1999).